Efficiency of the Summer Monsoon in Generating Streamflow within a Seasonally Snow-Dominated Headwater Basin of the Colorado River

Carroll Rosemary W.H.[1], Gochis David J[2], and Williams Kenneth Hurst[3]

[1]Desert Research Institute
[2]National Center for Atmospheric Research (UCAR)
[3]Lawrence Berkeley National Laboratory (DOE)

November 16, 2022

Abstract

The North American Monsoon occurs July-September bringing significant rainfall to Colorado River headwater basins. This rain may buffer streamflow deficiencies caused by reductions in snow accumulation. Using a data-modeling framework, we explore the importance of monsoon rain in streamflow generation over historic conditions in an alpine basin. Annually, monsoon rain contributes 18{plus minus}7% water inputs, generates 10{plus minus}6% streamflow and increases water yield 3{plus minus}2% the following year. The bulk of rain supports evapotranspiration in lower subalpine forests. However, rains have the potential to produce appreciable streamflow at higher elevations where soil storage, forest cover and aridity are low; and rebounds late season streamflow 64{plus minus}13% from simulated reductions in snowpack as a function of monsoon strength. Interannual variability in monsoon efficiency to generate streamflow declines with low snowpack and high aridity, implying the ability of monsoons to replenish streamflow in a warmer future with less snow accumulation will diminish.

Efficiency of the Summer Monsoon in Generating Streamflow within a Seasonally Snow-Dominated Headwater Basin of the Colorado River

Rosemary W.H. Carroll[1,4], David Gochis[2], and Kenneth H. Williams[3,4]

[1]Desert Research Institute, Reno, NV, [2]National Center for Atmospheric Research, Boulder, CO, [3]Lawrence Berkeley National Laboratory, Berkeley, CA,[4]Rocky Mountain Biological Lab, Gothic, CO

Corresponding author: Rosemary W.H. Carroll (rosemary.carroll@dri.edu)

Key Points:

- Monsoons generate 10±6% of annual streamflow while late spring snowfall delivers twice as much for the same water input.
- The influence of monsoons on streamflow is lessoned by evapotranspiration in the lower subalpine forest.
- Monsoon efficiency in generating streamflow decreases in years with low snow accumulation and high aridity.

Abstract

The North American Monsoon occurs July-September bringing significant rainfall to Colorado River headwater basins. This rain may buffer streamflow deficiencies caused by reductions in snow accumulation. Using a data-modeling framework, we explore the importance of monsoon rain in streamflow generation over historic conditions in an alpine basin. Annually, monsoon rain contributes 18±7% water inputs, generates 10±6% streamflow and increases water yield 3±2% the following year. The bulk of rain supports evapotranspiration in lower subalpine forests. However, rains have the potential to produce appreciable streamflow at higher elevations where soil storage, forest cover and aridity are low; and rebounds late season streamflow 64±13% from simulated reductions in snowpack as a function of monsoon strength. Interannual variability in monsoon efficiency to generate streamflow declines with low snowpack and high aridity, implying the ability of monsoons to replenish streamflow in a warmer future with less snow accumulation will diminish.

Plain Language Summary

Monsoon rains bring much needed summer moisture to the southwestern United States, but it remains unclear whether rains have a significant effect on streamflow in the snow-dominated headwaters of the Colorado River. Lack of understanding is largely due to the difficulty in measuring rain and snowfall in steep, mountainous basins, and the effect both have on seasonal plant consumption of water. Using a hydrological model populated with ground, airborne and synthesized climate data, we compare relative efficiency of monsoon rain to generate stream water over multiple decades. Monsoon rains deliver one-fifth of the basin's water and produce 10% the annual streamflow, with additions largely confined to the upper elevations of the watershed where soils are thin, water is plentiful, and forests are less abundant. In contrast, lower elevations contain dense aspen and conifer forests that consume monsoon rain and limit streamflow response. Subsequently, even strong monsoon events cannot fully replenish lost snow. Summer rains produce more streamflow during cooler years with large snow accumulation. This hints that streamflow from summer rain may diminish in a warmer future with less snow.

1 Introduction

Snowpack in mountain systems is declining worldwide with trends in snow loss expected into the future (Hock et al., 2019). Across the western United States (US), rising temperatures and changing precipitation patterns have decreased peak snow accumulation 15-30% since the mid-20th century (Mote et al., 2018), with the intensity and duration of these seasonal snow deficits increasing over the last 40 years (Huning & AghaKouchak, 2020). Reductions in snow cover produce a positive albedo feedback that results in higher air temperatures that promotes additional snowmelt (Hall, 2004; Ma et al., 2019). Rising temperatures can also drive larger soil evaporation and plant transpiration (evapotranspiration, ET) to reduce streamflow (Milly & Dunne, 2020). The Colorado River in the southwest US is dependent on 90% of its flow from the snow covered headwaters of Utah, Colorado and Wyoming (Jacobs, 2011) and is emblematic of these cascading feedbacks with 20% streamflow reductions projected by mid-21st century (Vano et al., 2012). The North American Monsoon (NAM) can bring significant rain to the region July to September (Sheppard et al., 2002) that has the potential to buffer streamflow deficiencies related to reductions in snowpack. Or the corollary, a lack of monsoon rain could potentially promote late summer streamflow depletions and the potential to influence soil moisture memory on streamflow generation in the subsequent water year. To date, the influence of monsoon rainfall on streamflow generation in high elevation, snow-dominated basins remains uncertain largely due to difficulty in predicting and quantifying precipitation and snowmelt across mountainous watersheds (Deems et al., 2006; Harpold et al., 2012) and the tight coupling of climate, vegetation and topography (Bales et al., 2006; Tennant, 2016; Tennant et al., 2017) that controls hydrologic partitioning between ET and runoff (Carroll et al., 2019).

To capture these complex processes to better understand streamflow generation efficiency from NAM rains, we combine light detection and ranging (LiDAR) derived snow depths, precipitation and vegetation raster maps, an observation network of weather and stream discharge stations and a hydrologic numerical model of an alpine headwater basin of the Colorado River. Using this data-model framework, we pose the following questions over a multi-decadal, historical period: (i) How efficient are monsoon rains in generating streamflow and what are the principal controls on this efficiency? (ii) Can monsoon rains mitigate stream depletions from reduced snowfall and how important are they in promoting streamflow the following year?

2 Site Description and Methods

The study site is the East River, Colorado (ER, 85km^2, Figure 1). Climate is continental subarctic. Snowmelt drives peak streamflow, typically occurring in early June and receding through the summer and fall. Observational networks related to snow and streamflow are described by others (Carroll *et al.*, 2018; Hubbard *et al.*, 2018; Carroll *et al.*, 2019) with station locations provided in Figure 1. ER elevations range from 2760 to 4065 m with pristine alpine/barren (26%), conifer (45%, spruce/fir), aspen (12%) and smaller coverages by shrubs, meadows and riparian conditions. Two Snow Telemetry (SNOTEL) stations reside in proximity of the ER (Figure 1, Schofield and Butte) with their period of record (1987-2019) capturing a wide range in snow accumulation and monsoon scenarios. Daily observations of solar radiation and snow depth are taken from four weather stations (Figure 1: SG, KP, JF and BB). Observed streamflow (years 2015-2019) are based on data from Carroll and Williams (2019) with subbasin characteristics provided in Table S1. In addition, observed daily streamflow at PH are regressed with the US Geological Survey (USGS) stream gauge (ID: 09112500) located 25 km downstream to approximate observed discharge over the entire simulation.

Hydrologic modeling builds upon previous work (Fang *et al.*, 2019; Carroll *et al.*, 2019) Daily water budgets are estimated with the USGS Precipitation-Modeling Runoff System (PRMS, Markstrom *et al.*, 2015). Water and energy are tracked within and between the atmosphere, plant, soil and groundwater and fluvial subcomponents of the watershed. The finite difference grid resolution is 100 m with elevations resampled from the USGS National Elevation Dataset. LANDFIRE (2015) is used to derive parameters of dominant cover type, summer and winter cover density, canopy interception characteristics for snow and rain and transmission coefficient for shortwave radiation. Climate forcing uses minimum and maximum daily temperature lapse rates defined by the two SNOTEL stations adjusted for aspect. Schofield snowfall is spatially distributed using LiDAR derived snow depth observations from the Airborne Snow Observatory (ASO, Painter *et al.*, 2016) flown 4 April 2016. Snow depths are converted to snow water equivalent (SWE) based on ground surveys and density modeling. Rainfall is spatially distributed using the monthly Parameter-elevation Relationships on

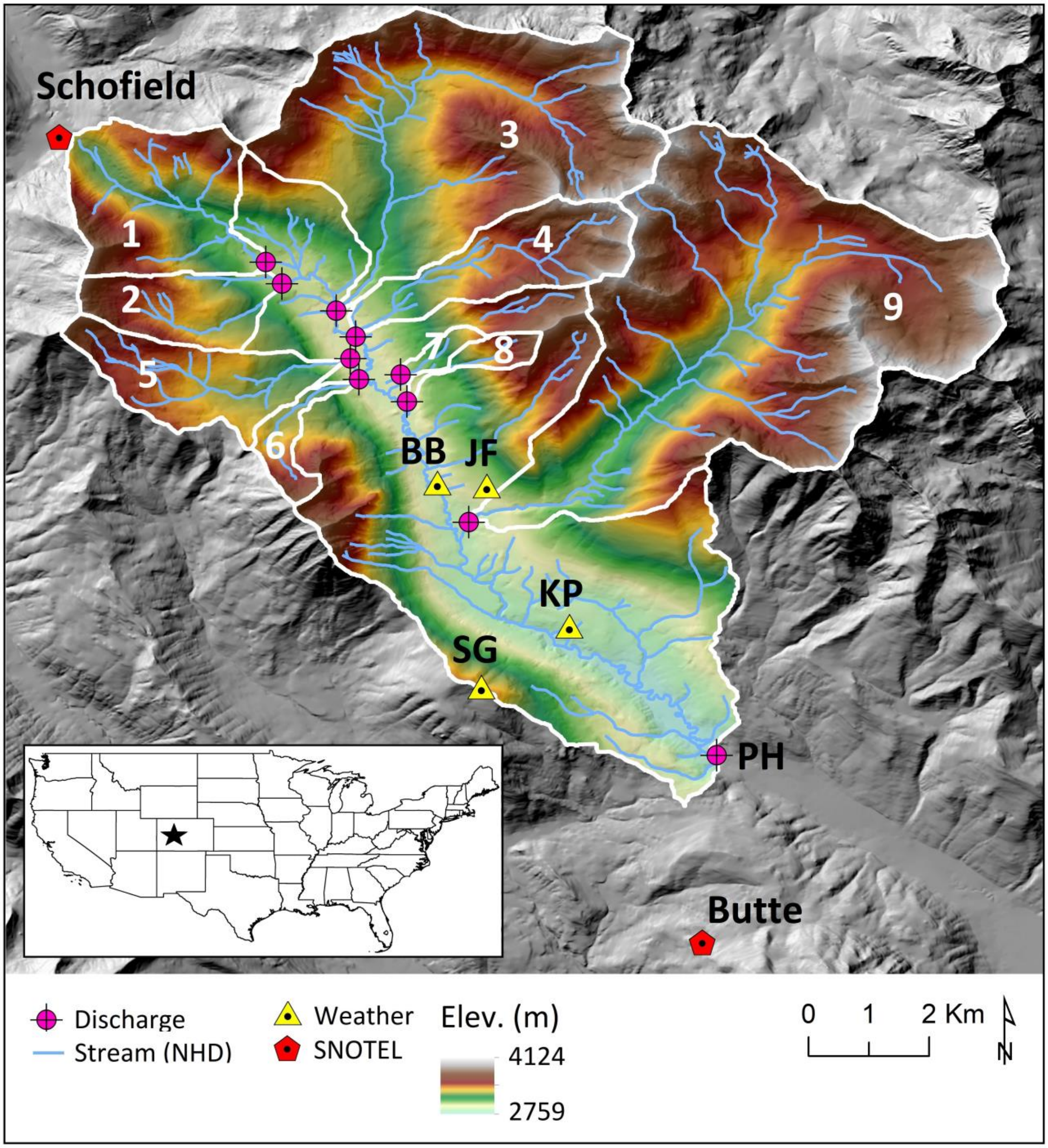

Figure 1. The East River and elevation with discharge, weather stations and sub-basins identified. Streams from the National Hydrographic Dataset (NHD). Sub-basin ID: 1 = East above Quigley (EAQ), 2 = Quigley, 3 = Rustlers, 4 = Bradley, 5 = Rock, 6 = Gothic, 7 = Marmot, 8 = Avery, 9 = Copper, PH = Pumphouse. Inset shows East River location in the continental United States.

Independent Slopes Model (PRISM, 800 m) 30-year (1981-2010) monthly averages (OSU, 2012) (Figure S1). Simulated solar radiation is calibrated to match weather station observations. Model verification of SWE accumulation and ablation relies on the 2018 and 2019 ASO maps and weather station snow depth.

Maximum soil water storage is conceptualized as a field capacity threshold above which water is partitioned to either shallow, lateral subsurface flow through the soil zone (interflow) or allowed to percolate downward via gravity drainage into the deeper groundwater system. The spatial distribution of soil storage is the product of rooting depth and available water content as a function of soil type (NRCS, 1991). Parameters related to solar radiation, potential evapotranspiration (PET), soil storage and groundwater transmissivity are adjusted at the subbasin level to best match observed solar radiation and stream discharge. Model sensitivity to seasonal precipitation is done by independently removing spring (April-May) or monsoon (July-September) water inputs. Precipitation is removed for a single year and changes in water budget components are compared to the historical (baseline) condition.

3 Results

Simulated daily solar radiation captures observed seasonal variability with a mean monthly relative root mean squared error (rrmse) of 6.4% (Figure S2). Modeled SWE replicates the spatial distribution of peak snow accumulation and late spring persistence during a dry year 2018, and peak accumulation in an extremely wet year 2019 (Figure S3); and mimics interannual variability of snow depth at the four weather stations (Figure S4). Annual average streamflow at all observed sites is modeled with rrmse of 2.4%. Daily flows (Figure S5) are well emulated for most of the subbasins with Nash Sutcliffe Efficiency (NSE) for EAQ = 0.57, Quigley = 0.38, Rustlers = 0.64, Rock = 0.66, and Copper = 0.67. PH has a NSE = 0.72 (log-flow NSE = 0.87) for directly observed data and 0.71 (log-flow 0.73) using the USGS regression. Average annual streamflow exiting the basin is 2.16±0.48 m^3/s (812± 204 mm/y) with flow highest in June (7.8±3.4 m^3/s) and lowest in February (0.42±0.19 m^3/s). Simulated precipitation is 1413±233 mm/y with 77±16% falling as snow. Total annual ET for the baseline simulation is 605±57 mm/y, or 43% total precipitation (P). ET components of sublimation, canopy evaporation and soil ET are estimated at 39±6 mm/y, 138±19 mm/y and 428±41 mm/y, respectively. Snow dominates water inputs October-May. Rain dominates June-August when conditions are typically water limited (PET>P). Otherwise the basin is predominantly energy limited (PET<P) (Figure S6). Monsoon precipitation is estimated 251±94 mm, or 18±7% annual water inputs with interannual rain anomalies oscillating over a 7-10year cycle with amplitude in anomalies increasing 50% since 2013 (Figure S7). On average, spring precipitation in April and May provide nearly equal inputs as the monsoon events (248±94 mm) though the interannual ratio is highly variable.

Several water budget components are collapsed to a single dimension (elevation) in Figure 2 for year 1998. Alpine conditions are defined above tree line (≥3750 m), while the subalpine is defined as conifer coverage ≥50% by area (3525-3000 m). Montane occurs at the lowest elevations where shrubs and aspen are dominant. Simulated SWE is largest in the alpine and upper subalpine. For 1998, late season snow (post-April 1) increases across most of the watershed by May 1, except at the lowest elevations where snowmelt exceeds any additional snowfall. By June 1, declines in SWE occur across all elevations with all snow melted in the montane. Interflow transports snowmelt downgradient with largest contributions into the upper subalpine. Snowmelt driven interflow increases water availability for ET (ET/PET increases) across all elevations with ET largest in the lower portions of the subalpine where conifer forests are most abundant, canopy density is highest, and aridity is slightly water limited. At lower elevations, water limiting conditions increase, lower snowpack and lower available interflow reduce water availability for ET such that ET begins to decline as a consequence. The removal of spring snow shifts water limited conditions to higher elevations compared to baseline. Interflow decreases below the alpine zone. Total ET increases in the alpine and upper subalpine and decreases in the lower portions of the subalpine and montane (refer to Figure S8 for changes in the spatial distribution of ET). Removal of monsoon rain reduces interflow above the upper subalpine but does increase aridity more in the lower subalpine and montane than removal of spring snow. ET and ET/PET decreases across all elevations, with ET decreasing the most in the lower subalpine.

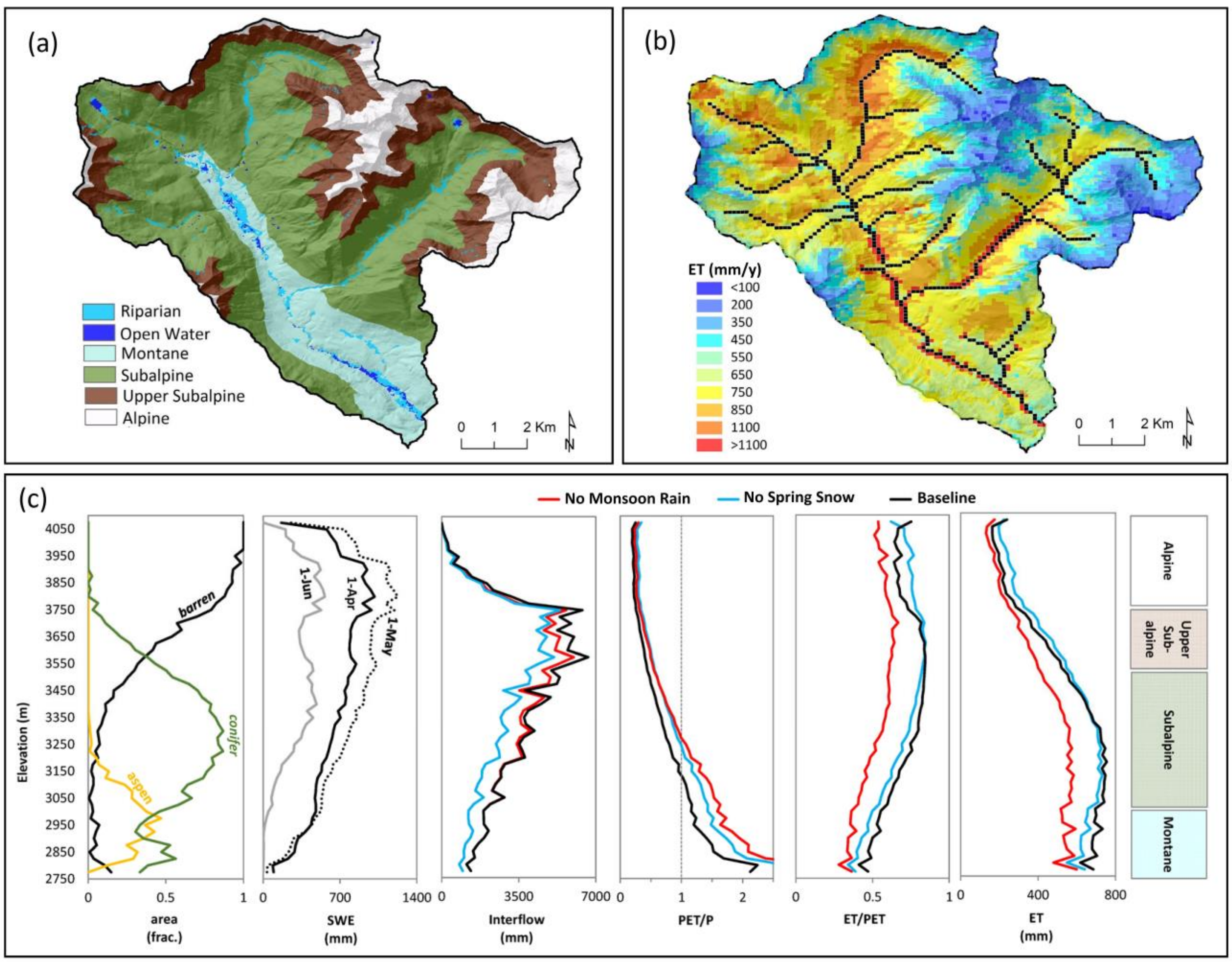

Figure 2. East River spatial trends in (a) ecosystems; and annual 1998 simulated (b) baseline evapotranspiration (mm/y) as well as elevation dependence of (c) area-weighted vegetation, snow water equivalent (SWE), interflow, aridity (PET/P), ET/PET and total ET. ‘No Monsoon Rain’ removes precipitation July–September, No Spring Snow removes precipitation April- May.

Daily water budgets for four different years illustrate the range in basin response to reduced seasonal water inputs (Figure S9). The largest snow accumulation occurred in 1995, with low PET and average monsoon conditions. Year 1998 had median snow accumulation, with below average but equal inputs of spring snow and monsoon rain. Year 2012 had the lowest snowfall and warmest conditions in the historical simulation. There was little spring snow but near normal monsoon conditions. Year 2018 was also a low snow year with warm conditions but had a monsoon nearly two standard deviations below normal. Loss of spring snow, with emphasis on average and above average snow accumulation years, promotes higher soil moisture early in the spring and earlier onset of ET and runoff. These effects are largely due to increases in PET through simulated feedbacks with increased solar radiation and the influence of reduced snow-covered area on albedo and faster snowmelt (Figure S10). Shortly thereafter, lost snowpack reduces soil moisture in comparison to baseline, but soil moisture is largely replenished by monsoon rains, and ET only declines in dry years with declines amplified in years with weak monsoons. Streamflow, however, drops below baseline in all scenarios and becomes reliant on groundwater (versus interflow) earlier in the year. Removal of monsoon rain also increases solar radiation and PET and experiences soil moisture and streamflow deficits in comparison to baseline.

A schematic of seasonal water partitioning for spring snow and monsoon rain is given in Figure S11, while controls on the ability of seasonal water inputs to generate streamflow is explored with simple regression analysis using annual totals in Figure 3. On average, monsoon rain contributes 10±6% to annual stream water. It is directly related to the amount of summer rain and is half as efficient at streamflow generation compared to spring snow for a given amount of water input. Monsoon rains support increases in basin scale ET (133±56 mm/y) and this is tightly controlled by the amount of rain. In contrast, increases in ET as a function of spring snow are much lower (31±27 mm/y) and this relationship declines with increases in contributing precipitation, albeit with a weak and insignificant trend ($p=0.24$). Sixty-five percent of the simulated variance in monsoon rain efficiency (streamflow generation per unit precipitation input) is described by peak SWE ($p<<0.01$) and PET ($p<0.01$), while sub-basin efficiency is best described by the indirect relationship of the forest areal coverage ($p=0.08$) and, to a lessor statistical degree, the canopy density ($p=0.18$). The ability for monsoon rain to generate streamflow in the following year (lag 1) is modest (3±2% increase), especially in comparison to spring snowfall's influence (22±17%). Increase in future flow due to monsoons rain is predominantly driven by the size of the monsoon ($r^2 = 0.44$, $p<<0.01$), but outlier years suggest the influence of monsoon rain increases when annual conditions are cool and PET is low ($r^2=0.33$, $p<<0.01$). A combined nonlinear function of total rain and PET describes 70% of simulated variability ($p<<0.01$) and is able to explain sharp increases in subsequent year streamflow generation approaching 8%. Lastly, the ability of monsoon rain to replace late season streamflow deficiencies (July-Dec.) as a consequence of reduced spring snowfall is 64±13%. Rebound in baseflow is directly related to the relative strength of monsoon inputs (R_s) defined as the ratio of monsoon rain to spring snowfall reduction ($p<<0.01$). Low R_s can only reduce deficiencies 33% while very large ratios (~2.5) allow an 83% recovery. By the end of December, monsoons replace streamflow deficiencies 87±7% with no monsoon scenario obtaining 100% streamflow recovery.

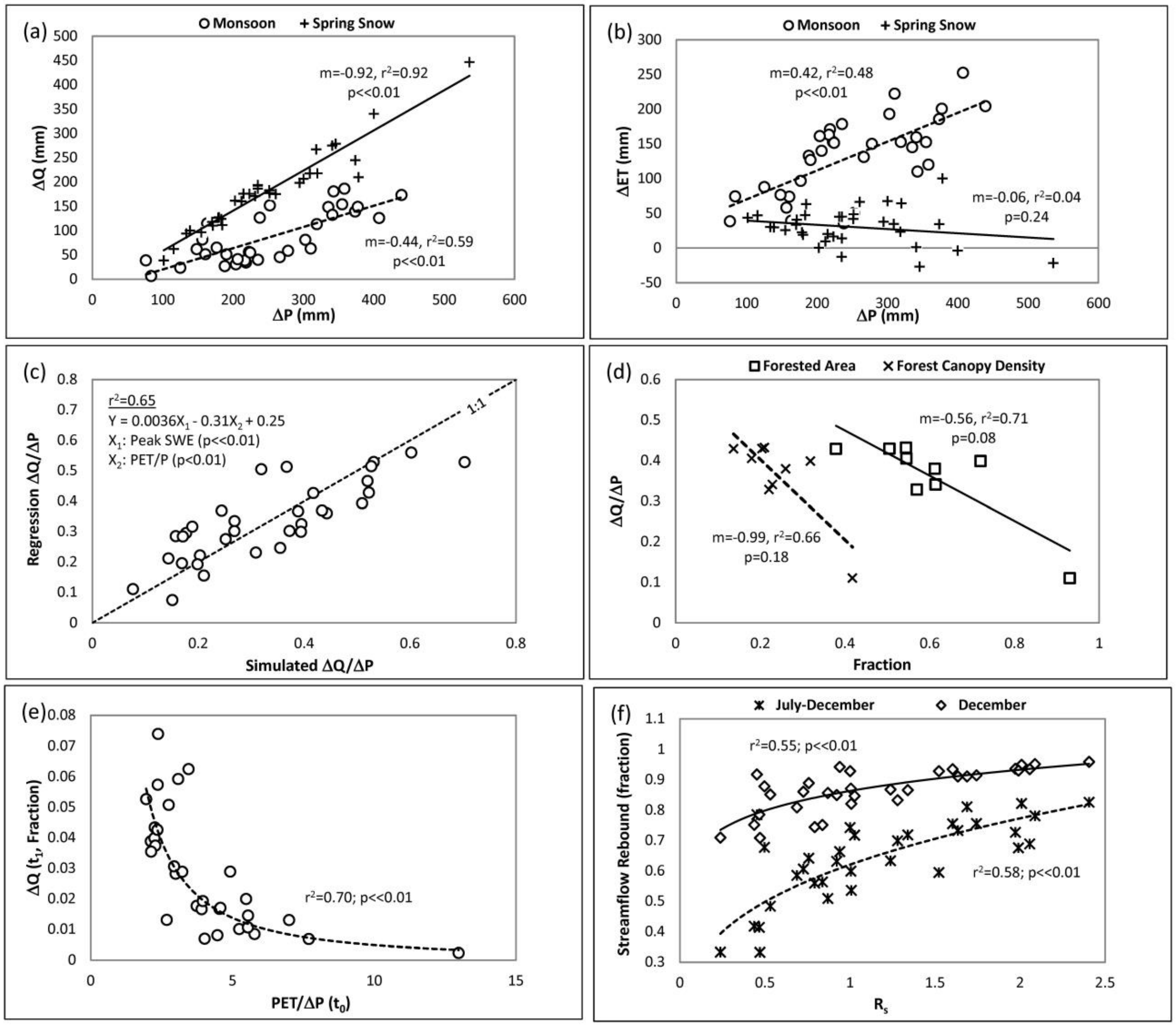

Figure 3. Annual water fluxes for 1987-2019. (a) Change in evapotranspiration (ΔET) as a function of added precipitation (ΔP) from spring snow (April-May) or monsoon rain (July-Sept). (b) Change in streamflow (ΔQ) for added precipitation. (c) Predictive ability of peak snow water equivalent (SWE) and aridity (PET/P) to describe numerical model simulated monsoon streamflow generation efficiency (ΔQ/ΔP). (d) Annual average efficiency for sub-basins in the East River as functions of forested area and forest canopy density. (e) Fractional increase in streamflow (lag 1, t_1) as a power function of potential ET (PET) and amount of monsoon rain (lag 0, t_0). (f) Fraction of streamflow rebound to baseline due to lost spring snow as a function of the ratio of monsoon precipitation to reduced spring snowfall (R_s).

4. Discussion

The timing and intensity of the NAM is dominated by large-scale atmospheric processes (Zhu et al., 2005) but influences of localized, land surface conditions (e.g. soil moisture) could be important. Several studies have suggested there is an inverse relationship between winter snow accumulation and summer rainfall with decreased snow accumulation driving reduced soil moisture such that less energy is needed to heat the land surface and this enhances the onset of rains (Gutzler, 2000; Lo & Clark, 2002; Zhu et al., 2005). In contrast, a positive soil moisture and rainfall feedback has been found by others (e.g. Vivoni, Tai and Gochis, 2009), while 470 years of precipitation records reconstructed with tree ring data found the historical inverse relationship between summer and winter precipitation weak and unstable despite appearing stronger during the latter half of the 20th century (Griffin et al., 2013). It is acknowledged the hydrologic model used in this analysis does not account for large scale ocean-atmospheric coupling nor soil moisture–atmospheric feedbacks. However, the use of local climate data from SNOTEL sites distributed with LiDAR derived SWE in combination with data reanalysis products, indicates that ER summer rain anomalies do not track sea temperature indices such as the Southern Oscillation Index (Trenberth, 2020) or Pacific Decadal Oscillation (Mantua, 2020), nor show a clear correlation to soil moisture. However, summer rains in the ER do show a statistically significant and indirect correlation with cumulative snow water inputs and PET. This suggests years with low snow accumulation and warm conditions might produce more summer rain, though the multiple regression's predictive power is low. Future work funded by the US Department of Energy's Atmospheric Radiation Measurement research program will, in part, focus on capturing precipitation phase, amount and intensity in the ER as well as investigate regional flow of water into the continental interior during the summer monsoon (https://www.arm.gov/news/facility/post/60749). This work will help better constrain where, when and how summer rains enter the ER.

A clearer coupling occurs between soil moisture and stream water generation. Initial conditions of soil moisture can improve streamflow forecasts (Crow et al., 2018; Mahanama et al., 2012; Shahrban et al., 2018). However, the sensitivity of ET and streamflow to soil moisture is a function of where the system resides on the spectrum between energy and water availability (Budyko, 1974; Orth & Seneviratne, 2013). PET, or the maximum amount of water transferred back to the atmosphere from the land surface if water is not limiting, is a commonly used metric to define energy availability. It varies seasonally as a function of temperature, solar radiation, vapor pressure and wind speed (ASCE, 2005). Likewise, water availability varies in space and time. Water availability prior to monsoon onset is largely dictated by the previous season's snow accumulation, redistribution and persistence (Hammond et al., 2018; Knowles et al., 2015) with these snow dynamics highly dependent on topography (Tennant et al., 2017) as well as vegetation type and structure (Bales et al., 2006; Broxton et al., 2015; Welch et al., 2016). Use of LiDAR snow observations accounts for where snow ends up, not necessarily where it fell. As such, the model implicitly accounts for snow redistribution by wind and avalanche as well as feedbacks between vegetation structure that may modify snow dynamics. Water availability also depends on lithologic and topographic characteristics that dictate water storage and holding capacity (Xiao et al., 2019) and the lateral redistribution of snowmelt via interflow (Carroll et al., 2019).

Research presented is largely inspired by exceptionally low NAM rain experienced in the ER 2018 and 2019 (z-score ~-2), and cited by regional water managers in Upper Colorado River for reducing late season flow to unprecedented levels (Sackett, 2018) and lowering streamflow forecasts the following year (Sackett, 2020). Because ET and streamflow are sensitive to energy and water availability and are highly co-dependent, it is important there is confidence that the hydrologic model captures these fluxes adequately for the baseline condition. The resultant, quasi-steady state water balance over multiple decades estimates annual ET equal to 605± 57 mm/y to balance incoming precipitation and outgoing streamflow. Streamflow is well constrained by observations; and snowfall, or the bulk of water inputs, is also constrained by observations. Estimated basin average ET is larger than eddy covariance flux tower data located near PH (417±29 mm/y) (Ryken et al., 2020), but is well aligned with Niwot Ridge eddy flux tower observations in a conifer (lodgepole) and aspen forest in Colorado (603 mm/y) (ameriflux.lbl.gov). Simulated ER seasonal variance encapsulates Niwot observations, but the model estimates lower median rates in the winter and higher rates in June (Figure S12). Likewise, modeled summer rates exceed those presented by (Ryken et al., 2020). Simulated summer rates are largely biased by the areally extensive subalpine where both energy and water availability are high. In contrast, reduced summer rates are simulated in portions of the basin where either energy (alpine) or water limited (montane) conditions occur that more closely resemble the flux tower data. With respect to winter ET, modeled snow losses, or the sum of sublimation and snow-only canopy evaporation, is 0.37-0.66 mm/d, or 17±9% of snowfall. Sexstone et al., (2016) reports lower total snow loss rates from open canopy at 0.36 mm/d in a Colorado basin, but losses are 15-17% total snowfall to suggest our winter ET estimates are reasonable.

Model results indicate monsoon rains generate 10±6% the annual streamflow total with these contributions helping to sustain late season baseflow. Results fall in the reported range of streamflow generated from rain across the western US at 30% (Li et al., 2017), and 1-2% (Julander & Clayton, 2018), with the lower limit occurring in more arid climates than the ER. Years with large snow accumulation and low atmospheric water demand directly describe the efficiency of monsoon rain to generate streamflow. Under these conditions, soil moisture holding capacity is exceeded for lower amounts of water input to allow more interflow, with a portion of interflow reaching stream channels. While snowmelt generated interflow occurs across all elevations, interflow from monsoon rain is largely constrained above treeline where soils are thin, and PET is low. Lower in the landscape, and along southern aspects, aridity (PET/P) is higher and is simulated more sensitive in solar radiation as a function of altering seasonal precipitation and inferred cloud cover. Sensitivity of PET to solar radiation in warmer conditions has been shown with similar, empirically-based methods (e.g. Priestley-Taylor) (Guo et al., 2017) to that used in PRMS (Jensen et al., 1969). These lower elevations, with emphasis in the subalpine forests, effectively eliminates streamflow response to monsoon rain through resulting increases in ET. In short, monsoon water inputs have a relatively small effect on streamflow through moderating effects of ET. Additionally, the ability of rain to generate streamflow is expected to decline in a future with less snow and warmer temperatures. In contrast, snowfall has a more complex relationship to ET in space and time driven by albedo-snowmelt feedbacks that substantively shift timing of melt and subsequent runoff (Barnett et al., 2005), but show relatively small net changes in ET compared to monsoon rains. The lower efficiency of ET to snowmelt is due to the timing of inputs prior to peak consumptive demand. This is supported by Berkelhammer et al. (2017) who found gross primary production (via satellite retrievals of solar-induced variability) in the intermountain west twice as sensitive to variations in rain compared to snow.

Despite differences in streamflow generation efficiencies, monsoon rain does help rebound baseflow deficiencies caused by a reduction snow accumulation. This ability is highly dependent on the relative strength of the monsoon, and no historical monsoon season can fully replenish streamflow deficits caused by hypothetical lost spring snowpack. This indicates that soil moisture dictated by snowmelt has long lasting effects on streamflow that cannot be fully reversed with summer rain. Likewise, soil moisture memory from summer rains is hypothesized to also impose on future streamflow. McNamara et al. (2005) finds remnant dry soils in the fall remain dry once snowfall commences, and these dry soils require more meltwater than wet soils to produce lateral movement of water in the spring. Thereby decreasing streamflow. Our model predicts monsoon memory on future streamflow, but this the effect is modest with average annual change to future flow only to 3±2%. Memory is controlled by the size of the monsoon and atmospheric water demand and shows no correlation to late season soil moisture. This lack of simulated response may be due to the simplistic soil conceptualization in the hydrologic model; or it may be thin soils in headwater basins are rewetted quickly by low quantities of snowmelt in comparison to the large quantities of snow available. These relationships may change as one moves down gradient in the Colorado River to warmer and drier climates, or if snow droughts continue to increase throughout the region to reduce snow accumulation in the ER. However, this requires a more detailed process-based investigation.

5 Conclusions

Summer rains are a critical water input to the ER with the amplitude of monsoon anomalies growing in the basin since 2013 and inspiring questions related to the efficiency of monsoon rains to generate streamflow. This is particularly important in the Colorado River Basin where snowpack is decreasing, and it is unknown if summer rains can buffer some of these losses. We find through a data-modeling framework that the efficiency of seasonal precipitation to produce streamflow is dictated by the timing of water input with respect to energy and water availability. Summer rains occur when PET is high and soil moisture is waning during the pre-monsoon drought. Subsequently, the bulk of rain serves to moisten very dry soils and does not generate interflow. Instead, water is quickly consumed by vegetation, with largest increases in ET occurring in the lower subalpine dominated by aspen and conifer forests. As a result, streamflow contributions from rain are half those generated by spring snowfall which occur when PET is low and soils moisture is higher. Most of the rain-generated streamflow occurs at higher elevations in the watershed where soil storage, forest cover and aridity are low. Summer rain does rebound late summer streamflow from simulated reductions in snowpack as a function of monsoon strength but is unable to fully replace streamflow from lost snow accumulation even for the largest historical monsoon event. Results do show memory of monsoon rains propagate into the following year through altered baseflow, but do not indicate memory as a function of fall soil moisture condition. Interannual variability in monsoon efficiency to generate streamflow declines when snowpack is low and aridity is high. This underscores the likelihood that the ability of monsoon rain to generate streamflow will decline in a warmer future with increased snow drought.

Acknowledgments and Data

Model characterization, validation and additional results are provided in the Supporting Information. Model input and output files are available to the public on the US Department of Energy (DOE) Environmental Systems Science Data Infrastructure for Virtual Ecosystem (ESS-DIVE DOI placeholder). Work is supported by the US DOE Office of Science under contract DE-AC02-05CH11231 as part of Lawrence Berkeley National Laboratory Watershed Function Science Focus Area. Additional support from Boise State University DOE contract DE-SC0019222.

References

ASCE. (2005). *The ASCE standardized reference evapotranspiration equation*, Technical Committee Report to the Environmental and Water Resources Institute of the American Society of Civil Engineers from the Task Committee on Standardization of Reference Evapotranspiration. https://www.mesonet.org/images/site/ASCEEvapotranspiration_Formula.pdf

Bales, R. C., Molotch, N. P., Painter, T. H., Dettinger, M. D., Rice, R., & Dozier, J. (2006). Mountain hydrology of the western United States. *Water Resources Research*, *42*(8), 1–13. https://doi.org/10.1029/2005WR004387

Bales, R., Molotch, N., Painter, T., Dettinger, M., Rice, R., & Dozier, J. (2006). Mountain hydrology of the Western United States. *Water Resources Research*, *42*, 1208. https://doi.org/doi:10.1029/2005WR004387

Barnett, T. P., Adam, J. C., & Lettenmaier, D. P. (2005). Potential impacts of a warming climate on water availability in snow-dominated regions. *Nature*, *438*, 303–309. https://doi.org/http://dx.doi.org/10.1038/nature04141.

Berkelhammer, M., Stefanescu, I. C., Joiner, J., & Anderson, L. (2017). High sensitivity of gross primary production in the Rocky Mountains to summer rain. *Geophysical Research Letters*, *44*(8), 3643–3652. https://doi.org/10.1002/2016GL072495

Broxton, P. D., Harpold, A. A., Biederman, J. A., Troch, P. A., Molotch, N. P., & Brooks, P. D. (2015). Quantifying the effects of vegetation structure on snow accumulation and ablation in mixed-conifer forests. *Ecohydrology*, *8*(6), 1073–1094. https://doi.org/10.1002/eco.1565

Budyko, M. I. (1974). *Climate and Life*. Elsevier.

Carroll, R.W.H., & Williams, K. H. (2019). Discharge data collected within the East River for the Lawrence Berkeley National Laboratory Watershed Function Science Focus Area (Water years 2015-2018). *ESS-DIVE*. https://doi.org/http://dx.doi.org/10.21952/WTR/1465929

Carroll, Rosemary W. H., Deems, J. S., Niswonger, R., Schumer, R., & Williams, K. H. (2019). The Importance of Interflow to Groundwater Recharge in a Snowmelt-Dominated Headwater Basin. *Geophysical Research Letters*, *46*(11), 5899–5908. https://doi.org/10.1029/2019GL082447

Carroll, Rosemary W.H., Bearup, L. A., Brown, W., Dong, W., Bill, M., & Willlams, K. H. (2018). Factors controlling seasonal groundwater and solute flux from snow-dominated basins. *Hydrological Processes*, *32*(14), 2187–2202. https://doi.org/10.1002/hyp.13151

Carroll, Rosemary W.H., Deems, J. S., Niswonger, R., Schumer, R., & Williams, K. H. (2019). The Importance of Interflow to Groundwater Recharge in a Snowmelt-Dominated Headwater Basin. *Geophysical Research Letters*, *46*(11), 5899–5908. https://doi.org/10.1029/2019GL082447

Crow, W. T., Chen, F., Reichle, R. H., Xia, Y., & Liu, Q. (2018). Exploiting Soil Moisture, Precipitation, and Streamflow Observations to Evaluate Soil Moisture/Runoff Coupling in Land Surface Models. *Geophysical Research Letters*, *45*(10), 4869–4878. https://doi.org/10.1029/2018GL077193

Deems, J. S., Fassnacht, S. R., & Elder, K. J. (2006). Fractal distribution of snow depth from LiDAR data. *Journal of Hydrometeorology*, *7*, 285–297.

Fang, Z., Carroll, R. W. H., Schumer, R., Harman, C., Wilusz, D., & Williams, K. H. (2019). Streamflow partitioning and transit time distribution in snow-dominated basins as a function of climate. *Journal of Hydrology*, *570*(December 2018), 726–738. https://doi.org/10.1016/j.jhydrol.2019.01.029

Griffin, D., Woodhouse, C. A., Meko, D. M., Stahle, D. W., Faulstich, H. L., Carrillo, C., Touchan, R., Castro, C. L., & Leavitt, S. W. (2013). North American monsoon precipitation reconstructed from tree-ring latewood. *Geophysical Research Letters*, *40*(5), 954–958. https://doi.org/10.1002/grl.50184

Guo, D., Westra, S., & Maier, H. R. (2017). Sensitivity of potential evapotranspiration to changes in climate variables for different Australian climatic zones. *Hydrology and Earth System Sciences*, *21*(4), 2107–2126. https://doi.org/10.5194/hess-21-2107-2017

Gutzler, D. S. (2000). Covariability of spring snowpack and summer rainfall across the Southwest United States. *Journal of Climate*, *13*(22), 4018–4027. https://doi.org/10.1175/1520-0442(2000)013<4018:COSSAS>2.0.CO;2

Hall, A. (2004). The role of surface albedo feedback in climate. *Journal of Climate*, *17*(7), 1550–1568. https://doi.org/10.1175/1520-0442(2004)017<1550:TROSAF>2.0.CO;2

Hammond, J. C., Saavedra, F. A., & Kampf, S. K. (2018). How does snow persistence relate to annual streamflow in mountain watersheds of the western U.S. with wet maritime and dry continental climates? *Water Resources Research*, *54*(4), 2605–2623. https://doi.org/doi:10.1002/2017WR021899

Harpold, A., Brooks, P., Rajagopal, S., Heidbuchel, I., Jardine, A., & Stielstra, C. (2012). Changes in snowpack accumulation and ablation in the intermountain west. *Water Resources Research*, *48*(11). https://doi.org/10.1029/2012WR011949

Hock, R., Rasul, G., Adler, C., Cáceres, B., Gruber, S., Hirabayashi, Y., Jackson, M., Kääb, A., Kang, S., Kutuzov, S., Milner, A., Molau, U., Morin, S., Orlove, B., & Steltzer, H. I. (2019). Chapter 2: High Mountain Areas. IPCC Special Report on the Ocean and Cryosphere in a Changing Climate. *IPCC Special Report on the Ocean and Cryosphere in a Changing Climate*, 131–202.

Hubbard, S. S., Williams, K. H., Agarwal, D., Banfield, J., Beller, H., Bouskill, N., Brodie, E., Carroll, R., Dafflon, B., Dwivedi, D., Falco, N., Faybishenko, B., Maxwell, R., Nico, P., Steefel, C., Steltzer, H., Tokunaga, T., Tran, P. A., Wainwright, H., & Varadharajan, C. (2018). The East River, Colorado, watershed: A mountainous community testbed for improving predictive understanding of multiscale hydrological–biogeochemical dynamics. *Vadose Zone Journal*, *17*(1). https://doi.org/10.2136/vzj2018.03.0061

Huning, L. S., & AghaKouchak, A. (2020). Global snow drought hot spots and characteristics. *Proceedings of the National Academy of Sciences*, 201915921. https://doi.org/10.1073/pnas.1915921117

Jacobs, J. (2011). Sustainability of Water Resources in the Colorado River Basin. *The Bridge: Linking Engineering and Society*, *41*((winter)), 6–12.

Jensen, M. E., Rob, D. C. N., & Franzoy, C. E. (1969). Scheduling irrigations using climate-crop-soil data. *National Conference on Water Resources Engineering of the American Society of Civil Engineers*, 20 p.

Julander, R. P., & Clayton, J. A. (2018). Determining the proportion of streamflow that is generated by cold season processes versus summer rainfall in Utah, USA. *Journal of Hydrology: Regional Studies*, *17*(December 2017), 36–46. https://doi.org/10.1016/j.ejrh.2018.04.005

Knowles, J. F., Harpold, A. A., Cowie, R., Zeliff, M., Barnard, H. R., Burns, S. P., Blanken, P. D., Morse, J. F., & Williams, M. W. (2015). The relative contributions of alpine and subalpine ecosystems to the water balance of a mountainous, headwater catchment. *Hydrological Processes*, *29*(22), 4794–4808. https://doi.org/10.1002/hyp.10526

LANDFIRE. (2015). *Existing vegetation type and cover layers*. U.S. Department of the Interior, Geological Survey. http://landfire.cr.usgs.gov/viewer/(accessed May 2017)

Li, D., Wrzesien, M. L., Durand, M., Adam, J., & Lettenmaier, D. P. (2017). How much runoff originates as snow in the western United States, and how will that change in the future? *Geophysical Research Letters*, 6163–6172. https://doi.org/10.1002/2017GL073551

Lo, F., & Clark, M. P. (2002). Relationships between spring snow mass and summer precipitation in the Southwestern United States associated with the North American monsoon system. *Journal of Climate*, *15*(11), 1378–1385. https://doi.org/10.1175/1520-0442(2002)015<1378:RBSSMA>2.0.CO;2

Ma, J., Zhang, T., Guan, X., Hu, X., Duan, A., & Liu, J. (2019). The dominant role of snow/ice Albedo feedback strengthened by black carbon in the enhanced warming over the Himalayas. *Journal of Climate*, *32*(18), 5883–5899. https://doi.org/10.1175/JCLI-D-18-0720.1

Mahanama, S., Livneh, B., Koster, R., Lettenmaier, D., & Reichle, R. (2012). Soil moisture, snow, and seasonal streamflow forecasts in the United States. *Journal of Hydrometeorology*, *13*(1), 189–203. https://doi.org/10.1175/JHM-D-11-046.1

Mantua, N. (2020). *Pacific Decadal Oscillation (PDO)*. http://research.jisao.washington.edu/pdo/PDO.latest

Markstrom, S. L., Regan, R. S., Hay, L. E., Viger, R. J., Webb, R. M. T., Payn, R. A., & LaFontaine, J. H. (2015). PRMS-IV, the precipitation-runoff modeling system, version 4. *U.S. Geological Survey Techniques and Methods, Book 6, Chap. B7*, 158. https://doi.org/http://dx.doi.org/10.3133/tm6B7

McNamara, J. P., Chandler, D., Seyfried, M., & Achet, S. (2005). Soil moisture states, lateral flow, and streamflow generation in a semi-arid, snowmelt-driven catchment. *Hydrological Processes*, *19*(20), 4023–4038. https://doi.org/10.1002/hyp.5869

Milly, P. C. D., & Dunne, K. A. (2020). *Colorado River flow dwindles as warming-driven loss of reflective snow energizes evaporation*. *9187*(February), 1–9.

Mote, P. W., Li, S., Lettenmaier, D. P., Xiao, M., & Engel, R. (2018). Dramatic declines in snowpack in the western US. *Npj Climate and Atmospheric Science*, *1*(1), 2. https://doi.org/10.1038/s41612-018-0012-1

NRCS. (1991). *Web Soil Survey*. United States Department of Agriculture. http://websoilsurvey.nrcs.usda.gov/accessed March 2016

Orth, R., & Seneviratne, S. I. (2013). Propagation of soil moisture memory to streamflow and evapotranspiration in Europe. *Hydrology and Earth System Sciences*, *17*(10), 3895–3911. https://doi.org/10.5194/hess-17-3895-2013

OSU. (2012). *PRISM Climate Group*. http://prism.oregonstate.edu

Painter, T. H., Berisford, D. F., Boardman, J. W., Bormann, K. J., Deems, J. S., Gehrke, F., Hedrick, A., Joyce, M., Laidlaw, R., Marks, D., Mattmann, C., McGurk, B., Ramirez, P., Richardson, M., Skiles, S. M. K., Seidel, F. C., & Winstral, A. (2016). The Airborne Snow Observatory: Fusion of scanning lidar, imaging spectrometer, and physically-based modeling for mapping snow water equivalent and snow albedo. *Remote Sensing of Environment*, *184*, 139–152. https://doi.org/10.1016/j.rse.2016.06.018

Ryken, A. E. C., Gochis, D., & Maxwell, R. (2020). Unraveling groundwater contributions to evapotranpiration in a mountain headwaters: Using eddy covariance to constrain water and energy fluxes in teh East River Watershed. *Authorea*. https://doi.org/10.22541/au.159559979.93668749

Sackett, H. (2018, October 2). Colorado's 2018 water year closes out as one of the driest on record. *Aspen Times*. https://www.aspentimes.com/news/local/colorados-2018-water-year-closes-one-of-driest-on-record/

Sackett, H. (2020, April 13). Streamflow forecast down for Roaring Fork despite above-normal snowpack. *Aspen Times*. https://www.aspentimes.com/news/streamflow-forecast-down-for-roaring-fork-despite-above-normal-snowpack/

Sexstone, G. A., Clow, D. W., Stannard, D. I., & Fassnacht, S. R. (2016). Comparison of methods for quantifying surface sublimation over seasonally snow-covered terrain. *Hydrological Processes*, *30*(19), 3373–3389. https://doi.org/10.1002/hyp.10864

Shahrban, M., Walker, J. P., Wang, Q. J., & Robertson, D. E. (2018). On the importance of soil moisture in calibration of rainfall–runoff models: two case studies. *Hydrological Sciences Journal*, *63*(9), 1292–1312. https://doi.org/10.1080/02626667.2018.1487560

Sheppard, P. R., Comrie, A. C., Packin, G. D., Angersbach, K., & Hughes, M. K. (2002). The climate of the US Southwest. *Climate Research*, *21*(3), 219–238. https://doi.org/10.3354/cr021219

Tennant, C. (2016). *Laser vision : LiDAR illuminates the influence of climate , topography , and vegetation on seasonal snowpack*.

Tennant, C. J., Harpold, A., Lohse, K. A., Godsey, S. E., Crosby, B. T., Larsen, L. G., Brooks, P. D., Van Kirk, R. W., & Glen, N. F. (2017). Regional sensitivities of seasonal snowpack to elevation, aspect, and vegetation cover in western North America. *Water Resources Research*. https://doi.org/10.1002/2016/WR019374

Trenberth, K. (2020). *The Climate Data Guide: Southern Oscillation Indices: Signal, Noise and Tahiti/Darwin SLP (SOI)*. https://climatedataguide.ucar.edu/climate-data/southern-oscillation-indices-signal-noise-and-tahitidarwin-slp-soi.

Vano, J. A., Das, T., & Lettenmaier, D. P. (2012). Hydrologic Sensitivities of Colorado River

Runoff to Changes in Precipitation and Temperature. *Journal of Hydrometeorology*, *13*(3), 932–949. https://doi.org/10.1175/JHM-D-11-069.1

Vivoni, E. R., Tai, K., & Gochis, D. J. (2009). Effects of initial soil moisture on rainfall generation and subsequent hydrologic response during the North American monsoon. *Journal of Hydrometeorology*, *10*(3), 644–664. https://doi.org/10.1175/2008JHM1069.1

Welch, C. M., Stoy, P. C., Rains, F. A., Johnson, A. V., & Mcglynn, B. L. (2016). The impacts of mountain pine beetle disturbance on the energy balance of snow during the melt period. *Hydrological Processes*, *30*(4), 588–602. https://doi.org/10.1002/hyp.10638

Xiao, D., Shi, Y., Brantley, S. L., Forsythe, B., DiBiase, R., Davis, K., & Li, L. (2019). Streamflow Generation From Catchments of Contrasting Lithologies: The Role of Soil Properties, Topography, and Catchment Size. *Water Resources Research*, *55*(11), 9234–9257. https://doi.org/10.1029/2018WR023736

Zhu, C., Lettenmaier, D. P., & Cavazos, T. (2005). Role of antecedent land surface conditions of North American monsoon rainfall variability. *Journal of Climate*, *18*(16), 3104–3121. https://doi.org/10.1175/JCLI3387.1

Geophysical Research Letters

Supporting Information for

Efficiency of the Summer Monsoon in Generating Streamflow within a Seasonally Snow-Dominated Headwater Basin of the Colorado River

Rosemary W.H. Carroll[1,4], David Gochis[2], and Kenneth H. Williams[3,4]

[1]Desert Research Institute, Reno, NV. [2]National Center for Atmospheric Research, Boulder, CO [3]Lawerence Berkeley National Laboratory, Berkeley, CA, [4]Rocky Mountain Biological Lab, Gothic, CO.

Contents of this file

Introduction

Additional East River (ER) model parameterization, calibration and output given in tabular and graphical form. Tables and figures are described in the main manuscript.

S.1. Hydrologic Model Parameterization

Table S1. East River sub-basin characteristics (modified from Carroll *et al.*, 2018)

Basin ID	name	Area[a]	Elev[b]	Relief[b]	Slope[b]	Aspect[b]	Annual Precip.[c]	Peak SWE[c]	Vegetation Type[d]			Total Forest[d]	Tree Density[e]
									Barren	Conifer	Aspen		
1	EAQ	5.27	3349	900	24	127	1,513	893	0.25	0.58	0.04	0.62	23
2	Quigley	2.55	3380	915	22	85	1,513	1,010	0.23	0.61	0.01	0.61	26
3	Rustlers	14.78	3490	1,118	22	196	1,573	907	0.24	0.54	0.00	0.54	18
4	Bradley	3.82	3504	1,107	22	242	1,502	917	0.41	0.50	0.00	0.51	20
5	Rock	3.57	3375	931	16	119	1,537	926	0.08	0.72	0.00	0.72	32
6	Gothic	0.90	3379	875	20	164	1,516	923	0.23	0.70	0.00	0.70	33
7	Marmot	0.38	3152	544	18	232	1,436	668	0.02	0.87	0.06	0.93	42
8	Avery	0.60	3390	916	28	243	1,321	687	0.34	0.52	0.02	0.54	21
9	Copper	23.67	3528	1,242	25	199	1,355	867	0.50	0.36	0.02	0.38	14
10	Pumphouse	84.73	3346	1,364	21	175	1,413	984	0.27	0.48	0.09	0.57	22

[a] km^2

[b]mean values for elevation (m), slope (%) and aspect (degrees); relief (m)

[c]simulated annual mean (mm) 1987-2019, SWE = snow water equivalent

[d]fraction of basin area

[e]area weighted fraction

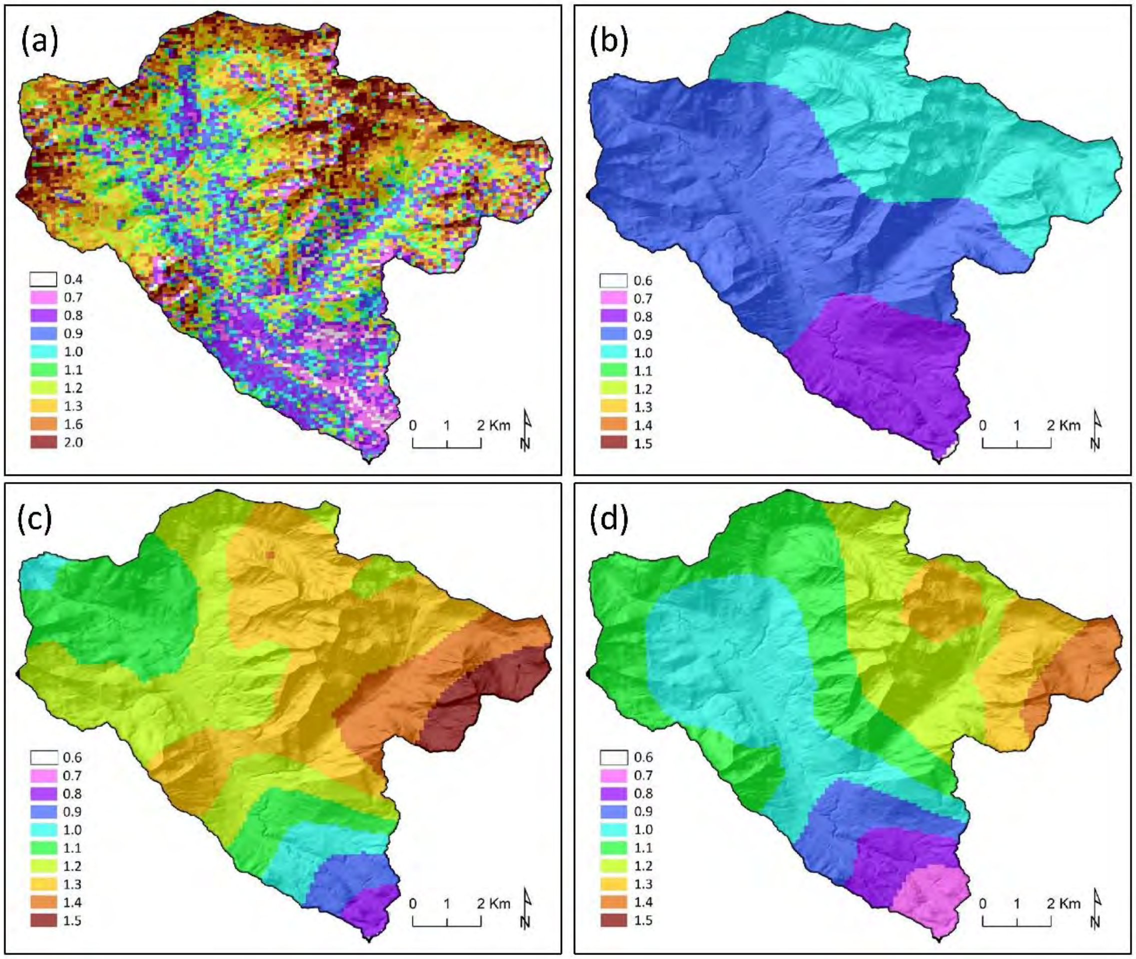

Figure S1. Ratios used to spatially distribute Schofield (a) snow water with ratios determined using snow water equivalent derived from LiDAR snow depths obtained during peak snow water equivalent on an average snow year April 4, 2016 (Painter et al., 2016) and adjusted for snow losses and melt prior to flight; and rain based on monthly average 30-year (1981-2010) PRISM raster maps (800 m) (OSU, 2012) (b) July, (c) August and (d) September.

S.2. Hydrologic Model Calibration and Verification

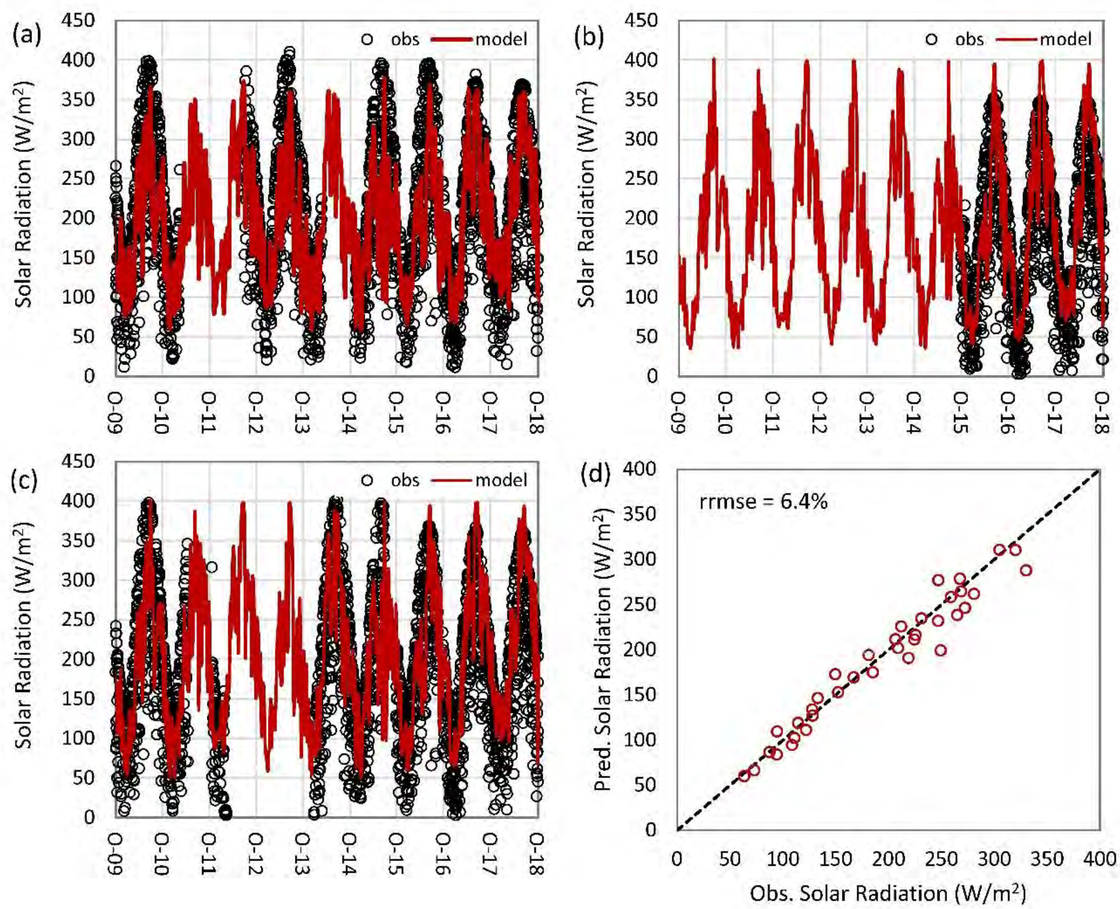

Figure S2. Updated simulated solar radiation results first presented by (Carroll et al., 2019). Observed and modeled solar radiation at Rocky Mountain Biological Laboratory (RMBL) weather stations (a) Kettle Ponds (KP), (b) billy barr (BB) and (c) Judd Falls (JF). Calibration accomplished adjusting the PRMS monthly degree-day slope parameter (dday_slope) to minimize the relative root mean squared error (rrmse) of mean monthly solar radiation at each station. Snodgrass (SG) not included in calibration. Model consistently over predicts this location by 125±33 W/m^2 with over prediction likely due to tall conifer forest (>10 m) encroaching on tower affecting observations. Locations provided in the manuscript Figure 1. Observed data available to the public at https://www.digitalrmbl.org/collections/weather-stations/.

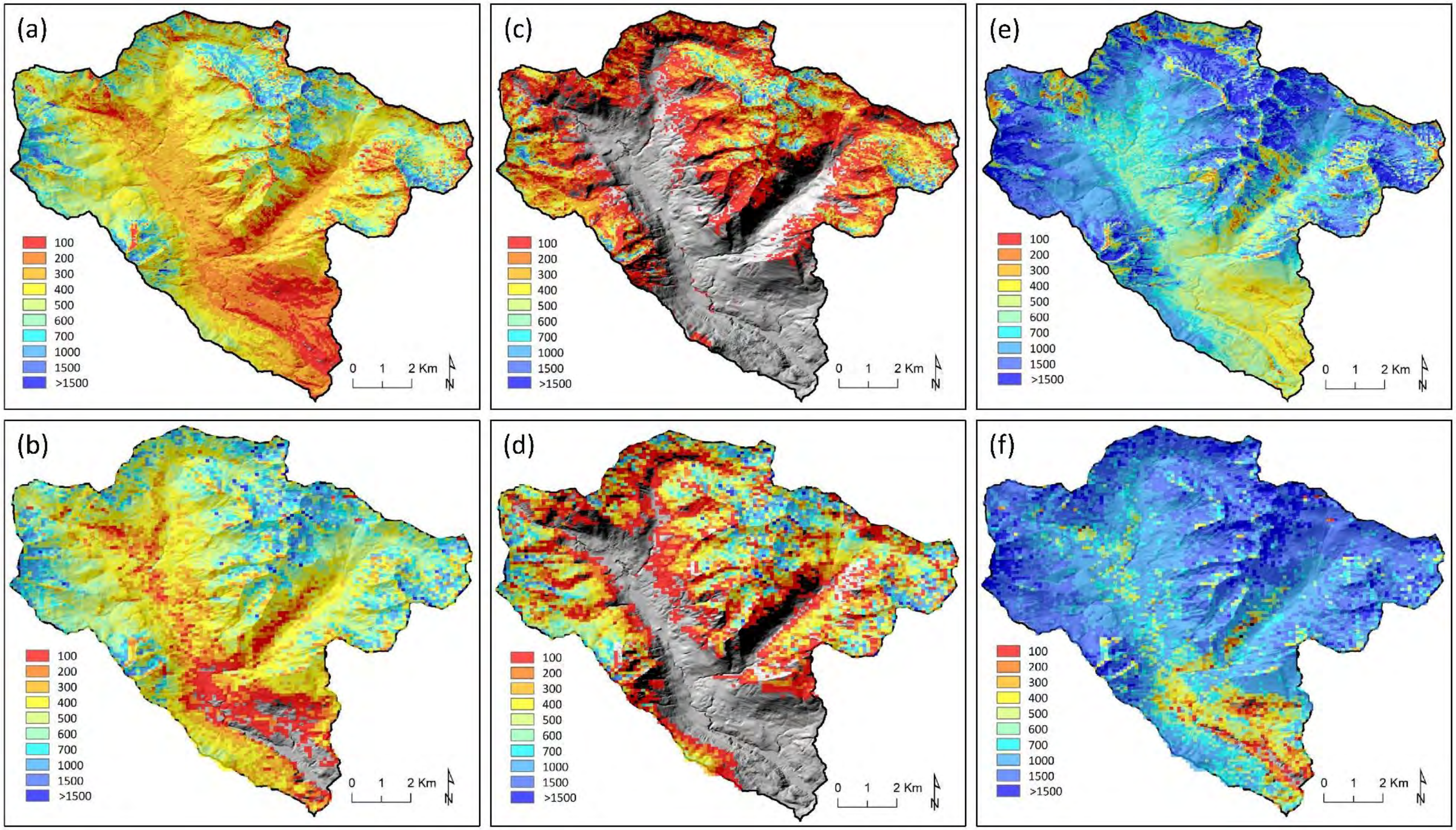

Figure S3. Validation of snow water equivalent (SWE, mm) between Airborne Snow Observatory (ASO, 50-m resolution) and PRMS (100-m resolution) for March 30, 2018 (a) ASO, (b) PRMS; May 24, 2018 (c) ASO and (d) PRMS, and April 7, 2019 (e) ASO, (f) PRMS

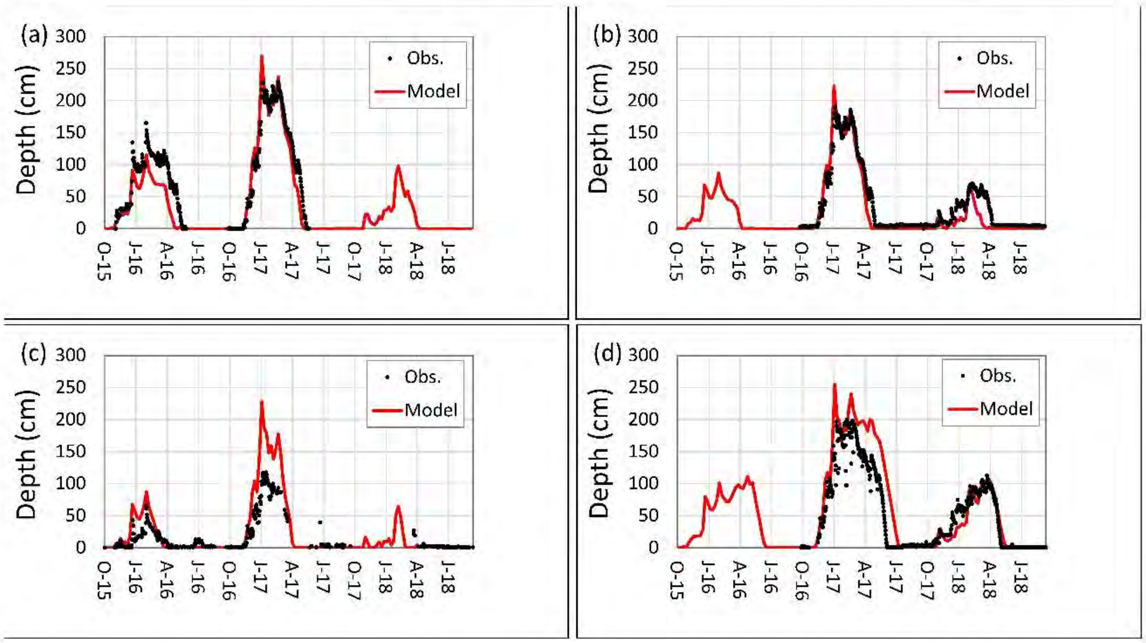

Figure S4. Snow depth comparison between observed weather stations and modeled, (a) billy barr (BB), (b) Judd Falls (JF), (c) Kettle Ponds (KP) and (d) Snodgrass (SG). Locations provided in the manuscript Figure 1. Simulated results updated from (Carroll et al., 2019). Observed data available to the public at https://www.digitalrmbl.org/collections/weather-stations/.

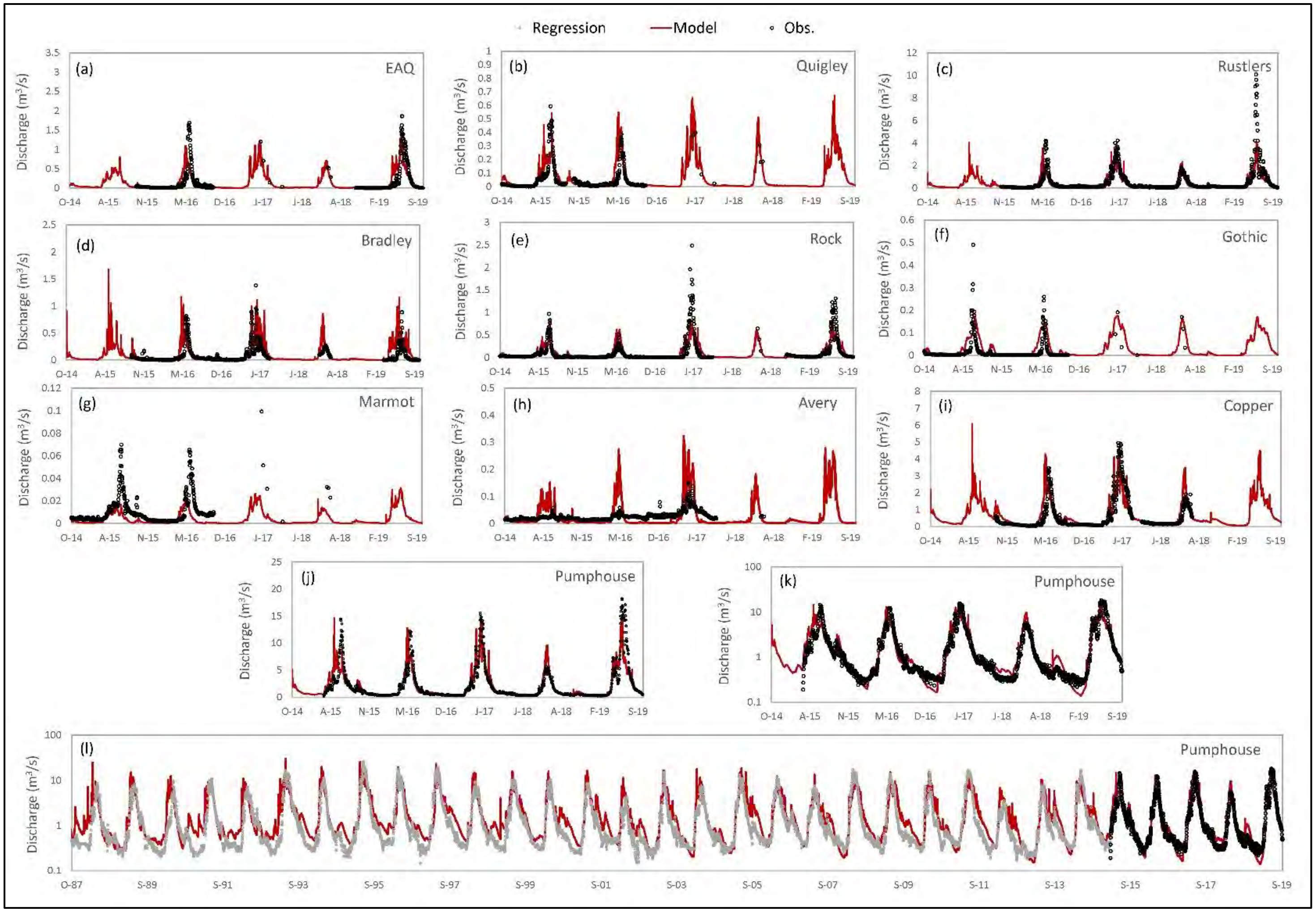

Figure S5. A comparison of daily observed and modeled streamflow for the period of record with data (a) EAQ, (b) Quigley, (c) Rustlers, (d) Bradley, (e) Rock, (f) Gothic, (g) Marmot, (h) Avery, (i) Copper, (j) Pumphouse, (k) Pumphouse, log streamflow and (l) Pumphouse log streamflow for entire simulation with estimated flow from USGS stream gauge (ID 09112500) located 25 km downstream.

S.3. Hydrologic Model Results

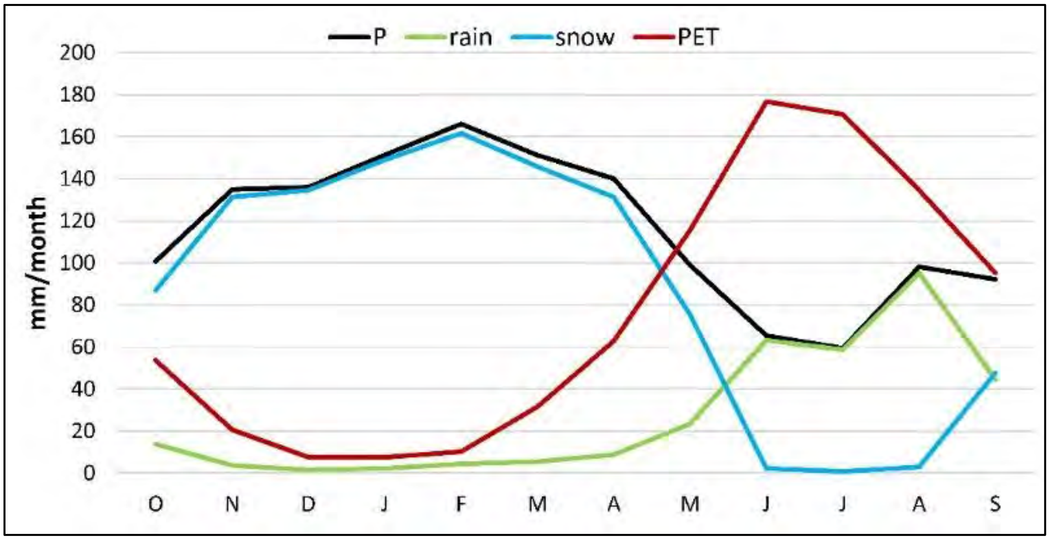

Figure S6. East River basin scale average simulated monthly precipitation (P) and potential evapotranspiration (PET). Precipitation is divided into rain and snow contributions

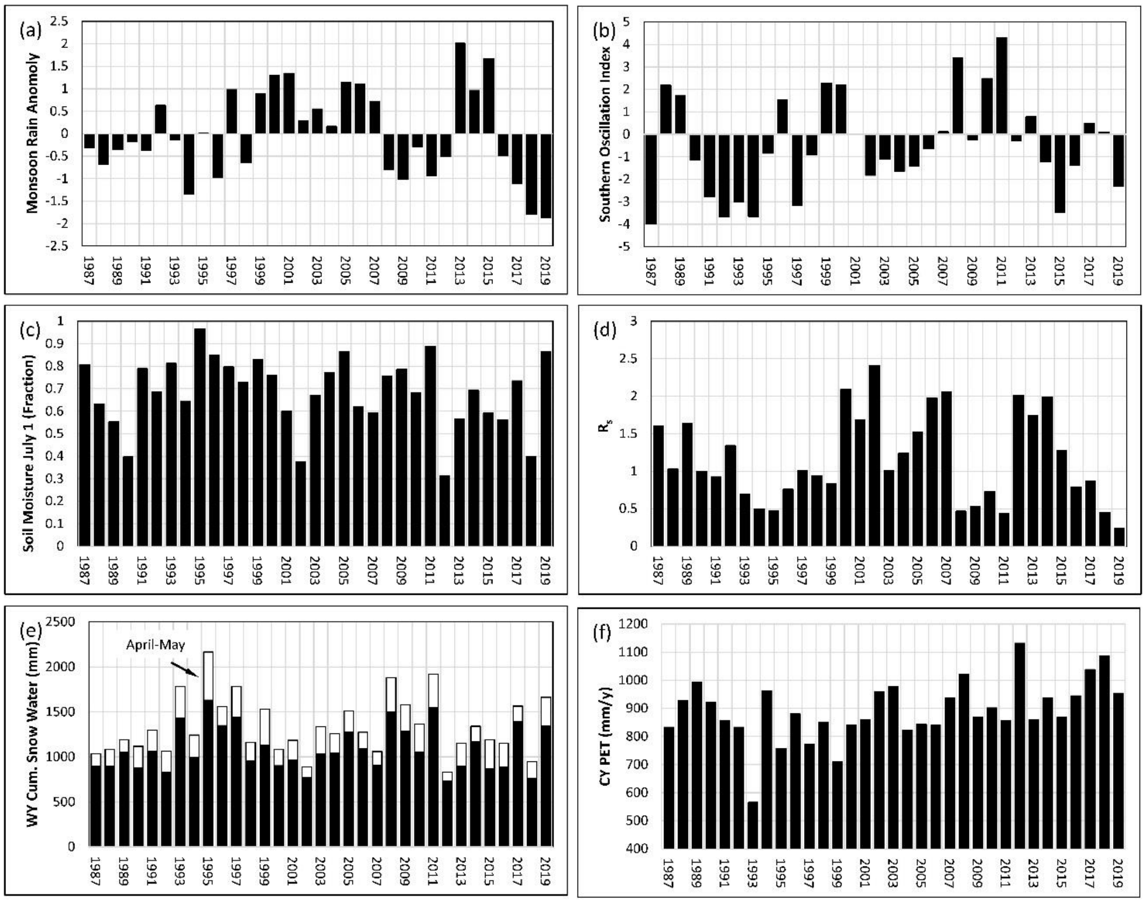

Figure S7. East River simulated (a) monsoon rain (July-September) anomalies (z-score), (b) Southern Oscillation Index (Trenberth, 2020), (c) soil moisture fraction July 1, (d) the ratio of monsoon rain to spring snowfall, R_s (c) water year (Oct-Sept) cumulative snow water input with the spring snow contributions in April and May identified, (d) calendar year potential evapotranspiration (PET).

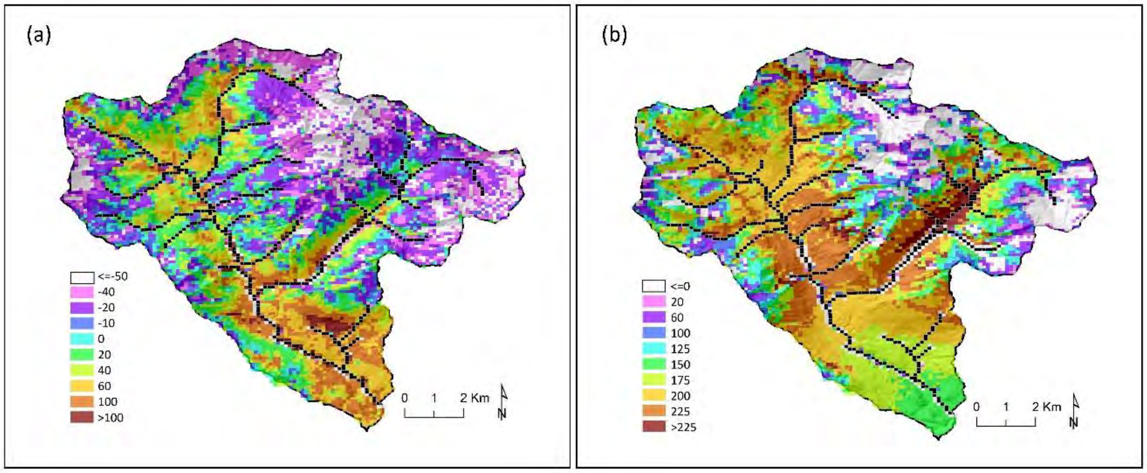

Figure S8. Spatial differences in 1998 annual total evapotranspiration (mm/y) defined as baseline – scenario for (a) no spring snow in April and May, (b) no monsoon rain July-September. Note that color code scale varies, and a negative value indicates an increase as a result of removing seasonal water input. Black model cells are simulated river cells.

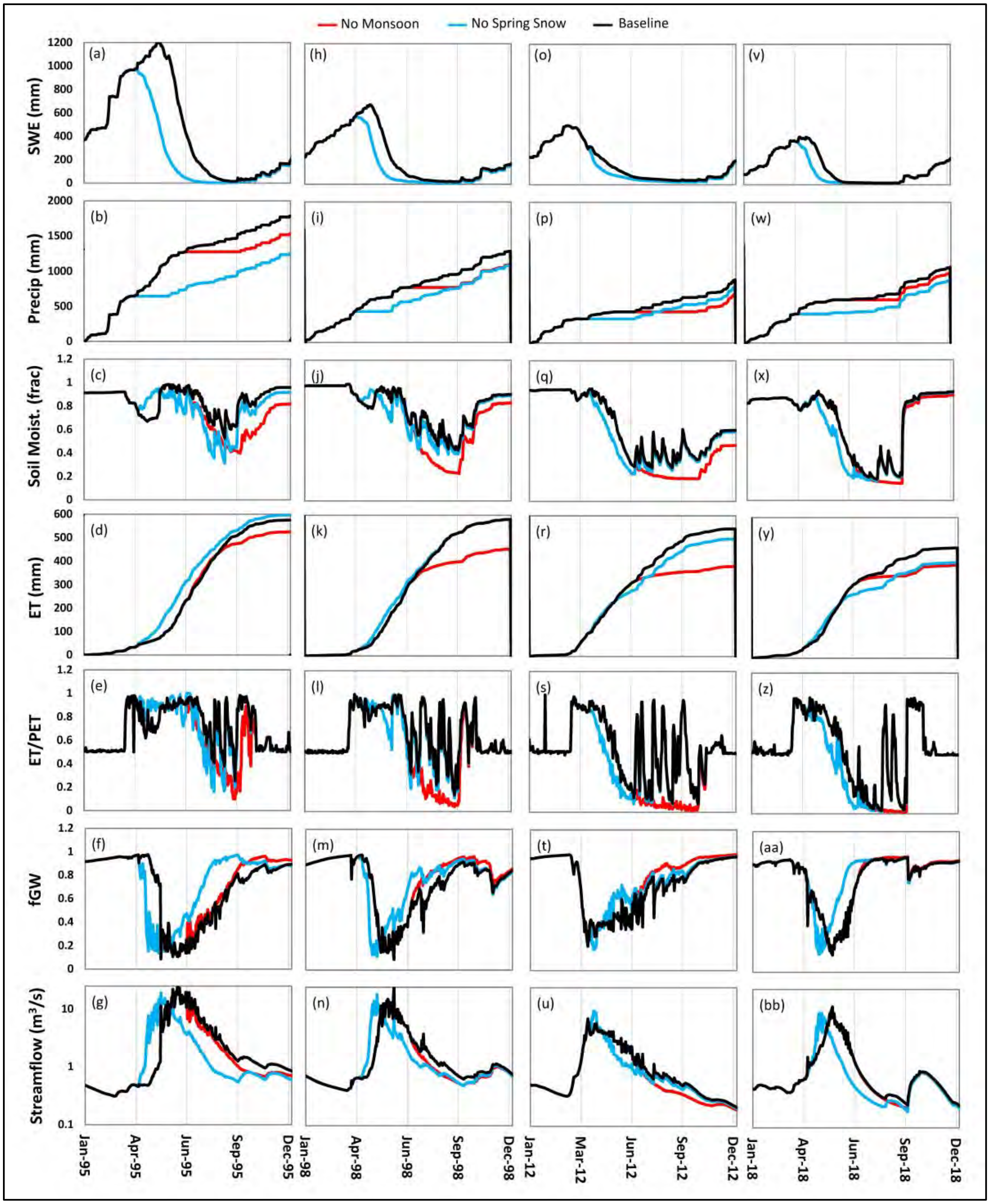

Figure S9. Simulated basin-scale daily water budget items for baseline and scenarios removing spring snow (April-May) and monsoon rain (July-September) for years: (a-g) 1995 (h-n) 1998, (o-u) 2012, and (v-bb) 2018. SWE = snow water equivalent, fGW = fraction of groundwater contributed to stream.

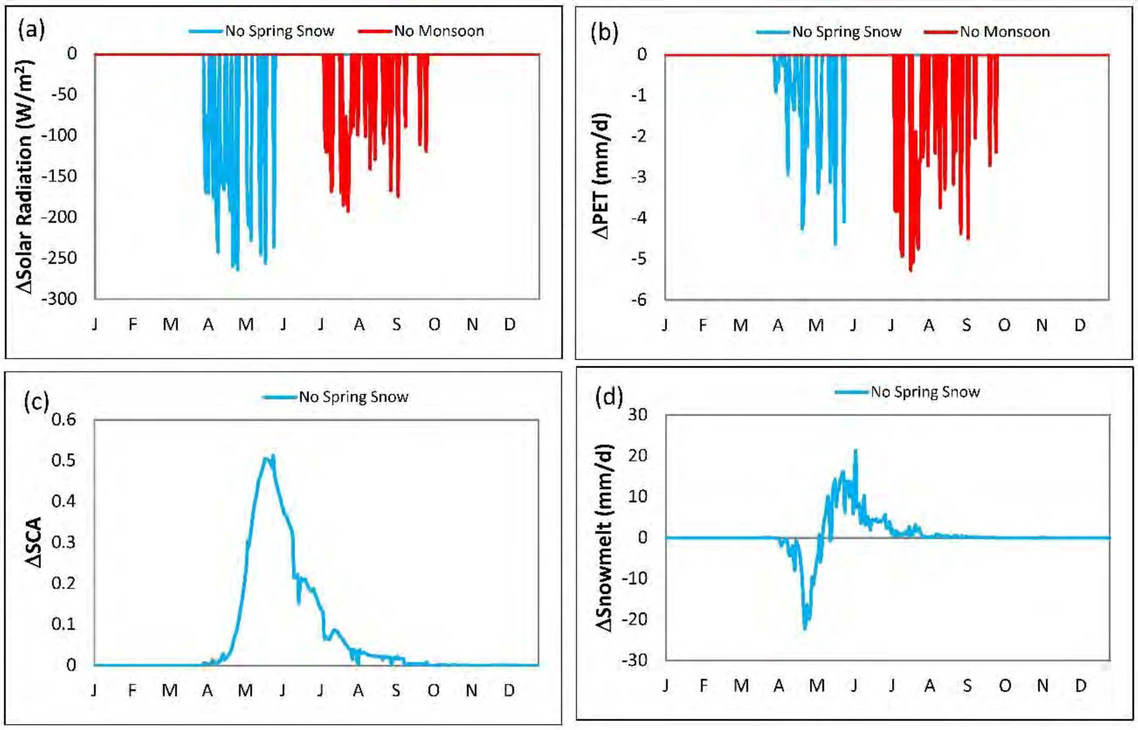

Figure S10. Temporal changes (Δ) for year 1998 between baseline and removal of either spring snow or monsoon rain: (a) solar radiation, (b) potential ET, PET, (c) snow covered area, SCA, and (d) snowmelt. For clarity, a negative value indicates increases as a result of removing seasonal water input.

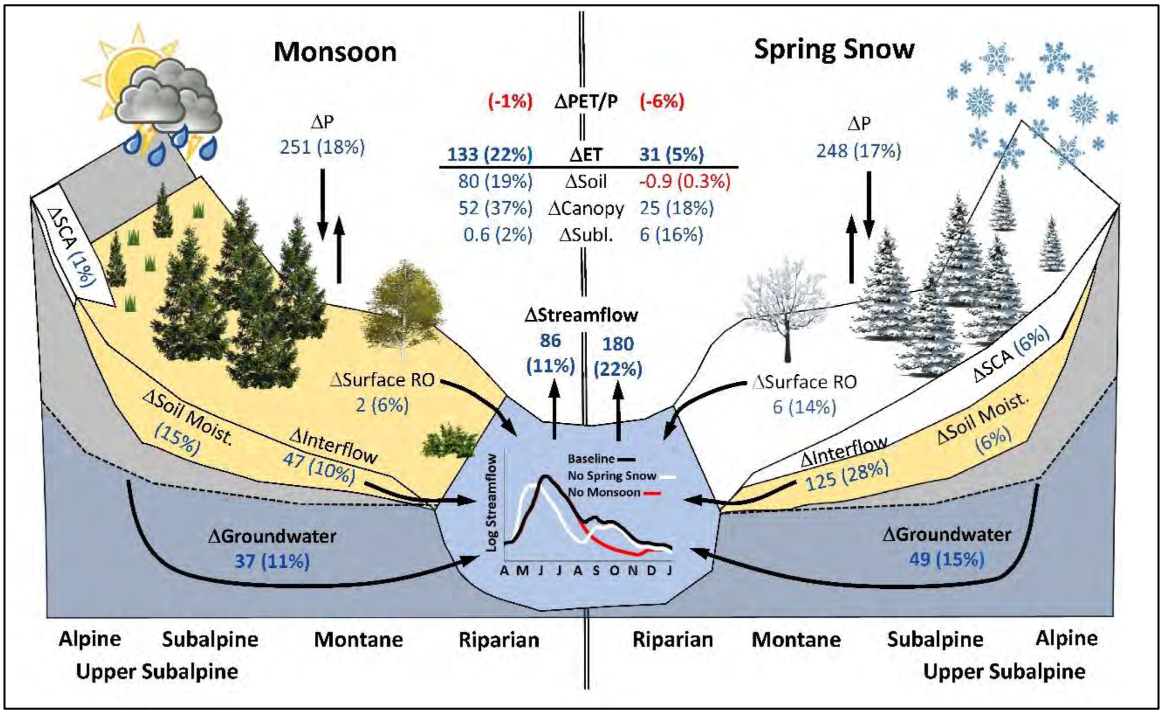

Figure S11. Average annual changes in water fluxes (and snow, soil storage) between the baseline (1987-2019) and scenarios with no monsoon (July-September) and no spring (April-May) precipitation. Blue (red) font = increase (decrease) due to added water input. SCA = snow covered area. RO = runoff.

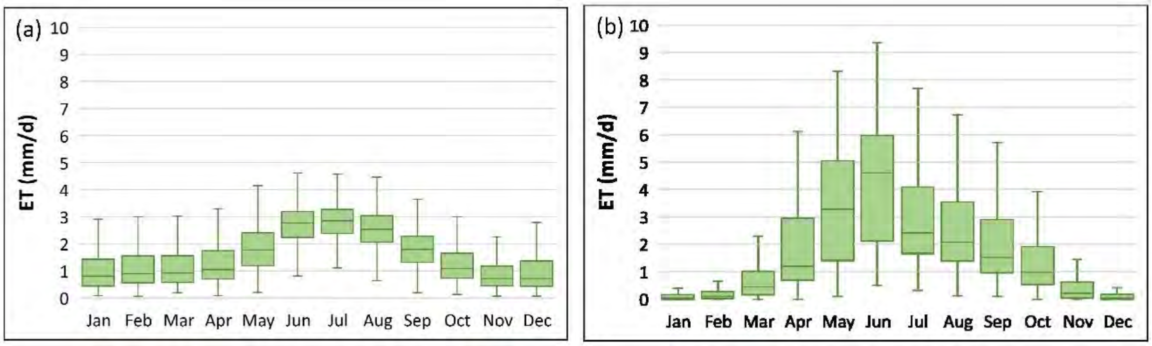

Figure S12. A comparison of average monthly evapotranspiration (ET) rates from daily aggregated totals for (a)Ameriflux stations Niwot Ridge LTER (US-NR1), years 1998-2019, (b) simulated with PRMS, years 1987-2019. Ameriflux 30-min latent heat flux data available at ameriflux.lbl.gov.

References Cited

Carroll, R. W. H., Bearup, L. A., Brown, W., Dong, W., Bill, M., & Willlams, K. H. (2018). Factors controlling seasonal groundwater and solute flux from snow-dominated basins. *Hydrological Processes*, *32*(14), 2187–2202. https://doi.org/10.1002/hyp.13151

Carroll, R. W. H., Deems, J. S., Niswonger, R., Schumer, R., & Williams, K. H. (2019). The Importance of Interflow to Groundwater Recharge in a Snowmelt-Dominated Headwater Basin. *Geophysical Research Letters*, *46*(11), 5899–5908. https://doi.org/10.1029/2019GL082447

OSU. (2012). *PRISM Climate Group*. http://prism.oregonstate.edu

Painter, T. H., Berisford, D. F., Boardman, J. W., Bormann, K. J., Deems, J. S., Gehrke, F., Hedrick, A., Joyce, M., Laidlaw, R., Marks, D., Mattmann, C., McGurk, B., Ramirez, P., Richardson, M., Skiles, S. M. K., Seidel, F. C., & Winstral, A. (2016). The Airborne Snow Observatory: Fusion of scanning lidar, imaging spectrometer, and physically-based modeling for mapping snow water equivalent and snow albedo. *Remote Sensing of Environment*, *184*, 139–152. https://doi.org/10.1016/j.rse.2016.06.018

Trenberth, K. (2020). *The Climate Data Guide: Southern Oscillation Indices: Signal, Noise and Tahiti/Darwin SLP (SOI)*. https://climatedataguide.ucar.edu/climate-data/southern-oscillation-indices-signal-noise-and-tahitidarwin-slp-soi. Data downloaded August 31, 2020